Orientational self-sorting in cuboctahedral Pd cages

Chemical Science

ROYAL SOCIETY OF CHEMISTRY

EDGE ARTICLE

View Article Online
View Journal | View Issue

Cite this: *Chem. Sci.*, 2022, **13**, 11912

All publication charges for this article have been paid for by the Royal Society of Chemistry

Received 11th July 2022
Accepted 29th September 2022

DOI: 10.1039/d2sc03856k

rsc.li/chemical-science

Orientational self-sorting in cuboctahedral Pd cages†

Ru-Jin Li,[a] Andrew Tarzia,[b] Victor Posligua,[b] Kim E. Jelfs,[b] Nicolas Sanchez,[c] Adam Marcus,[c] Ananya Baksi,[d] Guido H. Clever,[d] Farzaneh Fadaei-Tirani[a] and Kay Severin*[a]

Cuboctahedral coordination cages of the general formula $[Pd_{12}L_{24}]^{24+}$ (L = low-symmetry ligand) were analyzed theoretically and experimentally. With 350 696 potential isomers, the structural space of these assemblies is vast. Orientational self-sorting refers to the preferential formation of particular isomers within the pool of potential structures. Geometric and computational analyses predict the preferred formation of cages with a *cis* arrangement at the metal centers. This prediction was corroborated experimentally by synthesizing a $[Pd_{12}L_{24}]^{24+}$ cage with a bridging 3-(4-(pyridin-4-yl)phenyl)pyridine ligand. A crystallographic analysis of this assembly showed exclusive *cis* coordination of the 3- and the 4-pyridyl donor groups at the Pd^{2+} ions.

Introduction

Reactions of ditopic N-donor ligands L with Pd^{2+} ions can give molecularly defined nanostructures of the general formula $[Pd_nL_{2n}]^{2n+}$.[1] The structural diversity of these assemblies is remarkable, ranging from simple dinuclear $[Pd_2L_4]^{4+}$ complexes[1c] to interlocked $[Pd_4L_8]^{8+}$ cages[2] and giant $[Pd_{30}L_{60}]^{60+}$ and $[Pd_{48}L_{96}]^{96+}$ spheres.[3] The geometry of the ligand is a decisive factor for the assembly process, with the ligand bend angle (the relative orientation of the coordinate vectors) being of special importance.[1,4] Other factors such as ligand–ligand interactions[5] or template effects[6,7] can also influence the self-assembly process.

In terms of applications, different directions have been explored, including the use of $[Pd_nL_{2n}]^{2n+}$ complexes as receptors for ions and drugs,[8,9] as components of novel materials,[10] as reactors for chemical transformations,[11] and as links for nanoparticles.[12]

For future advances, it is desirable to extend the library of available $[Pd_nL_{2n}]^{2n+}$ nanostructures.[13] Given the importance of the ligand in the self-assembly process, it is clear that ligand design is key for generating new $[Pd_nL_{2n}]^{2n+}$ complexes. Most homoleptic $[Pd_nL_{2n}]^{2n+}$ complexes are based on ligands with identical N-donor groups, and these ligands typically display C_{2v} symmetry.[1]

The utilization of low-symmetry ligands with two distinct donor groups represents an attractive strategy to access new $[Pd_nL_{2n}]^{2n+}$ structures.[13,14] A potential problem of this approach is the formation of isomers. For $[Pd_2L_4]^{4+}$-type assemblies, the use of a low-symmetry ligand can give rise to four different isomers, which differ in the relative orientation of the ligands (Fig. 1).

Experimental studies have shown that the selective formation of one isomer with a particular relative orientation of the ligands is possible ('orientational self-sorting').[15] However, the energy difference between the isomers is sometimes not sufficient for providing a good selectivity.[15b,c]

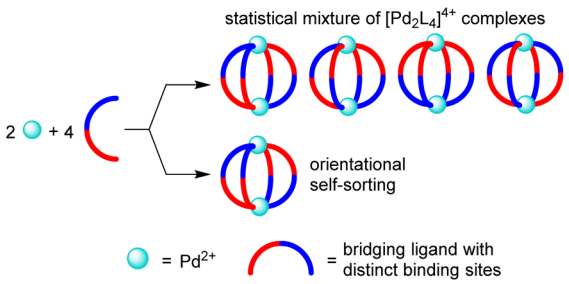

Fig. 1 The combination of a curved ligand L with two distinct binding sites (blue/red) and Pd^{2+} ions can lead to the formation of four different $[Pd_2L_4]^{4+}$ complexes. 'Orientational self-sorting' refers to the preferential formation of complexes with a particular relative orientation of the bridging ligand (the selective formation of the *cis* isomer is shown as a representative example).

[a]*Institut of Chemical Sciences and Engineering, École Polytechnique Fédérale de Lausanne (EPFL), Lausanne 1015, Switzerland. E-mail: kay.severin@epfl.ch*

[b]*Department of Chemistry, Molecular Sciences Research Hub, Imperial College London, White City Campus, 82 Wood Lane, London, W12 0BZ, UK*

[c]*Institut of Mathematics, EPFL, Lausanne 1015, Switzerland*

[d]*Fakultät für Chemie und Chemische Biologie, Technische Universität Dortmund, Universität Dortmund, Dortmund 44227, Germany*

† Electronic supplementary information (ESI) available: Containing synthetic procedures and experimental details. CCDC 2161290. For ESI and crystallographic data in CIF or other electronic format see https://doi.org/10.1039/d2sc03856k

For $[Pd_nL_{2n}]^{2n+}$ assemblies based on low-symmetry ligands, the number of potential isomers quickly increases with n. Macrocyclic $[Pd_3L_6]^{6+}$ assemblies can form 9 isomers, pseudo-tetrahedral $[Pd_4L_8]^{8+}$ complexes can form 35 isomers, and octahedral $[Pd_6L_{12}]^{12+}$ complexes can form 112 different isomers.[16,17] These numbers increase to 16, 68, and 186 if enantiomers are included.

Despite the vast number of potential isomers, orientational self-sorting is possible for high-nuclearity $[Pd_nL_{2n}]^{2n+}$ assemblies, as demonstrated by a recent experimental study from our group.[16] The utilization of a thiophenylene-spaced ligand with 3- and 4-pyridyl donor groups gave rise to a structurally defined $[Pd_6L_{12}]^{12+}$ complex.

Below, we analyze the structures and the potential isomers of cuboctahedral $[Pd_{12}L_{24}]^{24+}$ complexes ($n = 12$). Geometric and computational analyses predict the preferred formation of cages with exclusive *cis* coordination at the metal centers. This prediction was corroborated experimentally by synthesis and structural analysis of a $[Pd_{12}L_{24}]^{24+}$ cage with a bridging 3-(4-(pyridin-4-yl)phenyl)pyridine ligand.

Results and discussion

In order to determine the number of potential isomers for $M_{12}L_{24}$ structures based on low-symmetry ligands, we have used a standard mathematical counting argument related to the Orbit-Stabilizer Theorem.[18] Our algorithm uses the cycle decomposition of the hyperoctahedral group[19] to generate the collection of configurations with non-trivial symmetries and then uses the Orbit-Stabilizer Theorem[18] to obtain a relationship between the number of distinct configurations and the number of symmetries each configuration has. As the set we generate is substantially smaller than the set of all possible configurations, we are able to apply this method of counting to $M_{12}L_{24}$ whose number of ligands proves too large for previous (exhaustive) methods.[16] A more detailed description of the procedure is given in the (ESI, Section 4†).

Our analysis revealed that $M_{12}L_{24}$ cages can form 350 696 potential isomers if the bridging ligands display distinct donor groups (Fig. 2). The vast majority of these isomers are chiral (99.8%). If enantiomers are taken into account, the total number of isomers increases to 700 688. The calculations show that the structural space of M_nL_{2n}-type assemblies increases dramatically when going from $n = 6$ (octahedral cages, 112 isomers) to $n = 12$ (cuboctahedral cages, 350 696 isomers).

Cuboctahedral complexes of type $M_{12}L_{24}$ can be deconstructed into four M_6L_6 hexagons, with the metal centers having an occupancy of 50% (Fig. 5a). Let's consider the case, which is schematically depicted in Fig. 3b. The assemblies are based on ditopic ligands having the following general characteristics: the ligand is perfectly rigid, the donor groups are chemically distinct (red/blue), the coordinate vectors form an angle of 120°, and the distance between the donor atoms and the intersection of the coordinate vectors is not equal ($a \neq b$). When combined with metal ions which act as linear connectors, three different hexagons can be formed (**A**–**C**, Fig. 3b). There are three ways to build an $M_{12}L_{24}$ assembly from **A**, and the resulting complexes have O_h, S_6, and C_{4h} symmetry. Hexagons of type **B** show two types of metal centers: three M are connected to the red parts of the ligand, and three M′ are connected to the blue parts of the ligand. The three M′ are positioned closer to the center of the hexagon **B** than the three M. The alternation of M and M′ in hexagon **B** makes it impossible to combine them into an $M_{12}L_{24}$-type assembly. The symmetry of the hexagon **C**, on the other hand, allows for the construction of a distorted cuboctahedron with D_{2h} symmetry.

The analysis suggests that for ligands with a fixed bend angle of 120° and a pronounced difference between the distances a and b, orientational self-sorting should occur. The four preferred $M_{12}L_{24}$ isomers are shown in Fig. 3b. Obviously, the geometric analysis is based on perfectly rigid systems, and it does not account for the conformational flexibility of real molecular systems (*e.g.* variable coordinate vectors).

To investigate whether orientational self-sorting can be observed in $[Pd_{12}L_{24}]^{24+}$-type assemblies, we have examined the

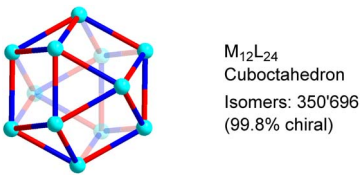

Fig. 2 Potential isomers for $M_{12}L_{24}$ cages with low-symmetry bridging ligands. The graphic shows only one of the possible isomers.

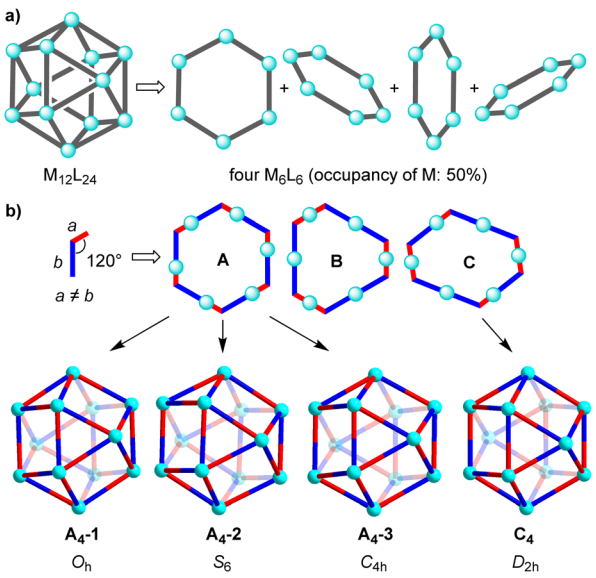

Fig. 3 (a) Deconstruction of an $M_{12}L_{24}$ assembly into four hexagons with a metal occupancy of 50%; (b) a ligand with two distinct donor groups (blue/red), a 120° angle between the coordinate vectors, and non-equal lengths a and b can form three different M_6L_6 hexagons (**A**–**C**). The construction of an $M_{12}L_{24}$ assembly can be achieved from hexagon **A** (three possible combinations) or from hexagon **C** (one possible combination), but not from **B** or from mixtures of **A**/**B**/**C**. For simplicity, the $M_{12}L_{24}$ isomers formed from **A** and **C** are depicted as ideal cuboctahedra with linear ligands.

reaction between $[Pd(CH_3CN)_4](BF_4)_2$ (a convenient source of Pd^{2+}) and ligand **L1** (Fig. 4a). This ligand was chosen because it displays a fixed bend angle of 120° (rotations around the C–C single bonds do not change the bend angle), and a pronounced difference between the distances of the N-donor atoms and the intersection of the coordinate vectors.

A mixture of $[Pd(CH_3CN)_4](BF_4)_2$ (1 equiv.) and **L1** (2 equiv.) in d_6-DMSO was tempered for 48 h at 70 °C. Subsequently, the resulting solution was analyzed by high-resolution ESI mass spectrometry and by NMR spectroscopy. The MS data confirmed the expected formation of a dodecanuclear assembly (Fig. 4b). The ^{1}H NMR spectrum showed broad peaks (Fig. 4c), which is expected for assemblies of this size.[1] A detailed analysis by ^{1}H–^{1}H COSY and NOESY correlation spectroscopy revealed three sets of signals for the protons of ligands **L1** (see the ESI, Fig. S9 and S10†). The three sets of signals have equal intensity, and the DOSY NMR spectrum (Fig. S11†) showed that they all belong to a species with the same diffusion constant. Overall, the NMR data suggested that the self-assembly process had resulted in the formation of one main species, rather than a complex mixture of isomers.

It is interesting to compare the NMR data with the results of the geometric analysis. The latter had predicted a preference for four isomers. Only two of the isomers have a ligand multiplicity of three, namely the C_{4h} symmetric isomer **A$_4$-3**, and the D_{2h} symmetric isomer **C$_4$** (ESI, Fig. S25†).

Expanding on the geometrical analysis depicted in Fig. 3, a computational study was performed in order to evaluate the relative stabilities of the four isomers **A$_4$-1**, **A$_4$-2**, **A$_4$-3**, and **C$_4$** of complex $[Pd_{12}(\mathbf{L1})_{24}]^{24+}$. Using an approach similar to recent work on Pd_2L_4 structures formed from low-symmetry ligands,[20] models of the four cages were constructed with the help of our Python framework, *stk*.[21,22] The geometry was optimized using a sequence of methods of increasing computational cost (see the ESI, Section 5†). Structures were optimized using UFF4MOF in GULP,[23] the semiempirical tight-binding method GFN2-*x*TB,[24] and, finally, density functional theory (DFT) geometry optimizations using hybrid and screened-hybrid functionals, PBE0-D3BJ[25] and HSE06,[26] respectively, with the Def2-SVP[27] basis set. Fig. 5 shows the relative energy of the isomers at the HSE06 level of theory, with **A$_4$-3** being the most stable isomer. However, the energy differences between the three **A$_4$** isomers are very small. In fact, the relative energy of the **A$_4$** isomers changes depending on the level of theory (see the ESI, Table S3†). Therefore, the calculations do not provide a significant distinction between the **A$_4$** isomers. However, the preference for **A$_4$** over **C$_4$** is apparent with an energy difference larger than 150 kJ mol^{-1}. This difference is significant, even if the limitations of our method (no solvent, no anions) are taken into account.

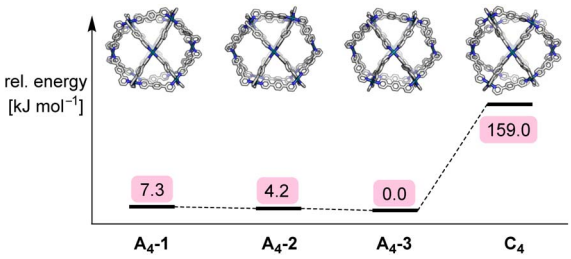

Fig. 5 Schematic of the relative energy differences of the four isomers **A$_4$-1**, **A$_4$-2**, **A$_4$-3**, and **C$_4$** of complex $[Pd_{12}(\mathbf{L1})_{24}]^{24+}$, along with graphics of the HSE06/Def2-SVP-optimized structures.

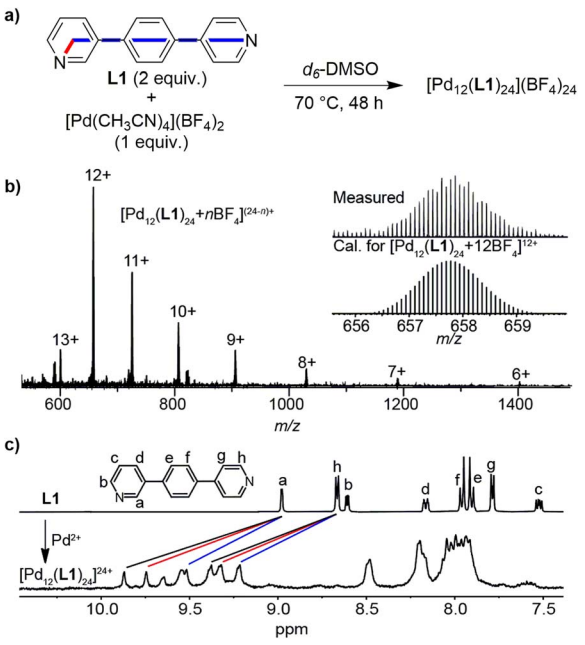

Fig. 4 (a) Synthesis of the coordination cage $[Pd_{12}(\mathbf{L1})_{24}](BF_4)_{24}$; (b) high-resolution ESI mass spectra of $[Pd_{12}(\mathbf{L1})_{24} + n BF_4]^{(24-n)+}$ (n) = 11–18); (c) ^{1}H NMR spectrum (d_6-DMSO) of the ligand **L1** (top) and of cage $[Pd_{12}(\mathbf{L1})_{24}](BF_4)_{24}$ (bottom).

To determine the structure of cage $[Pd_{12}(\mathbf{L1})_{24}]^{24+}$, a crystallographic analysis was needed. Obtaining good-quality diffraction data turned out to be challenging, but we finally succeeded in using single crystals obtained by vapor diffusion of THF/Et_2O into a solution of the cage in DMSO.[28] Co-crystallized solvent molecules could not be located, and the solvent-mask procedure from *Olex2* (ref. 29) was used to account for residual electron density. The structure of the polycationic cage could clearly be established (Fig. 6). The 12 Pd^{2+} all show a *cis* configuration, and the cage displays an approximate C_{4h} symmetry. Consequently, it is one of the four structures, which were predicted by the geometric analysis (**A$_4$-3**, Fig. 3b). The observed symmetry matches the signal multiplicity in the ^{1}H NMR spectrum (3 sets of signals), suggesting that the main structure in solution is the same as the one observed crystallographically. The presence of small amounts of other isomers cannot be excluded.

Cuboctahedral cages of the formula $[Pd_{12}L_{24}]^{24+}$ are typically observed for ligands with a bend angle of around 120°.[1,30] Further straightening of the ligand to bend angles between 134° and 149° can give rhombicuboctahedral $[Pd_{24}L_{48}]^{48+}$ cages.[1,4,31] $[Pd_{24}L_{48}]^{48+}$ cages can form up to 5.86 trillion isomers if low-symmetry ligands are employed (ESI,

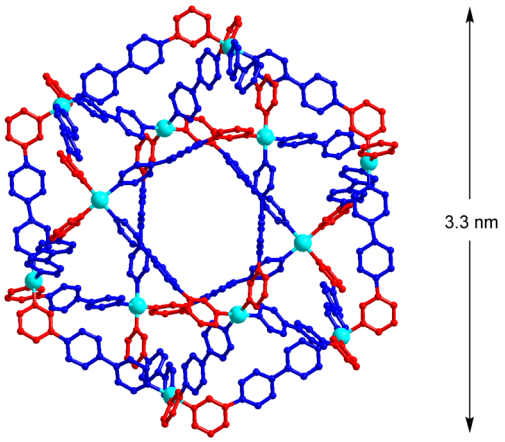

Fig. 6 Molecular structures of $[Pd_{12}(\mathbf{L1})_{24}]^{24+}$ as determined by X-ray crystallography. Hydrogen atoms and counter ions are not depicted. The color-coding of the ligand atoms aims to visualize the non-symmetric nature of the ligand.

Section 4†). A geometric analysis suggests that there is again a geometric preference for cages with *cis*-coordination at the metal centers (ESI, Section 3.3†). Preliminary attempts were made to examine orientational self-sorting in rhombicuboctahedral $[Pd_{24}L_{48}]^{48+}$ cages, but the available analytical data did not provide information about the selectivity of the assembly process. The interested reader can find more information in the ESI (Fig. S19–S21†).

Conclusions

Cuboctahedral coordination cages of the general formula $[Pd_{12}L_{24}]^{24+}$ (L = low-symmetry ligand) can potentially form 350 696 isomers, which differ in the relative orientation of the ligands. A geometric analysis combined with a computational study suggested the preferential formation of cages with *cis* coordination at the metal centers. Experimentally, we observed indeed the formation of a cage with *cis*-coordinated metal centers when Pd^{2+} salts were combined with 3-(4-(pyridin-4-yl) phenyl)pyridine.

The preference for *cis* coordination mirrors what we had observed for octahedral assemblies of type $[Pd_6L_{12}]^{12+}$ (L = low-symmetry ligand).[16] In fact, a geometrical analysis analogous to that shown in Fig. 3 predicts that *cis* coordination should be favored for $[Pd_6L_{12}]^{12+}$ cages (ESI, Section 3.2†).

Overall, our results substantiate that it is possible to obtain structurally defined $[Pd_nL_{2n}]^{2n+}$ cages of high nuclearity with low-symmetry ligands. A prerequisite for orientational self-sorting is the geometry of the ligand, which should display distinct distances between the donor atoms and the intersection of the coordinate vectors. Ligands of this kind will favor the formation of cages with a *cis* arrangement at the metal centers. We expect that the results of our analysis can be transferred to other types of coordination cages, given that donor groups of the ligands are coordinated in a square planar fashion to the metal centers.[32]

Data availability

The computational data is freely available at: **https://github.com/andrewtarzia/citable_data/tree/master/li_2022**

Author contributions

R.-J. L. and K. S. initiated the study, R.-J. L. performed the experiments and analyzed the data, A. T., V. P. and K. E. J. performed a computational analysis of the stability of $[Pd_{12}(\mathbf{L1})_{24}]^{24+}$ cages, N. S. and A. M. computed the potential isomers, A. B. and G. H. C were responsible for the MS measurements of cage $[Pd_{24}(\mathbf{L1})_{48}](BF_4)_{48}$, F. F.-T. collected and processed the X-ray data, and R.-J. L. and K. S. co-wrote the manuscript. All authors discussed the results and commented on the manuscript.

Conflicts of interest

There are no conflicts to declare.

Acknowledgements

The work was supported by the Swiss National Science Foundation, and by the École Polytechnique Fédérale de Lausanne (EPFL). KEJ thanks the Royal Society for a University Research Fellowship and the European Research Council through Agreement No. 758370 (ERC-StG-PE5-CoMMaD).

References

1 (*a*) T. Tateishi, M. Yoshimura, S. Tokuda, F. Matsuda, D. Fujita and S. Furukawa, *Coord. Chem. Rev.*, 2022, **467**, 214612; (*b*) N. B. Debata, D. Tripathy and H. S. Sahoo, *Coord. Chem. Rev.*, 2019, **387**, 273–298; (*c*) S. Saha, I. Regeni and G. H. Clever, *Coord. Chem. Rev.*, 2018, **374**, 1–14; (*d*) M. Han, D. M. Engelhard and G. H. Clever, *Chem. Soc. Rev.*, 2014, **43**, 1848–1860; (*e*) K. Harris, D. Fujita and M. Fujita, *Chem. Commun.*, 2013, **49**, 6703–6712.

2 M. Frank, M. D. Johnstone and G. H. Clever, *Chem.–Eur. J.*, 2016, **22**, 14104–14125.

3 (*a*) D. Fujita, Y. Ueda, S. Sato, H. Yokoyama, N. Mizuno, T. Kumasaka and M. Fujita, *Chem*, 2016, **1**, 91–101; (*b*) D. Fujita, Y. Ueda, S. Sato, N. Mizuno, T. Kumasaka and M. Fujita, *Nature*, 2016, **540**, 563–566.

4 Q.-F. Sun, J. Iwasa, D. Ogawa, Y. Ishido, S. Sato, T. Ozeki, Y. Sei, K. Yamaguchi and M. Fujita, *Science*, 2010, **328**, 1144–1147.

5 For examples, see: (*a*) J. Tessarolo, H. Lee, E. Sakuda, K. Umakoshi and G. H. Clever, *J. Am. Chem. Soc.*, 2021, **143**, 6339–6344; (*b*) B. Chen, J. J. Holstein, S. Horiuchi, W. G. Hiller and G. H. Clever, *J. Am. Chem. Soc.*, 2019, **141**, 8907–8913; (*c*) B. Chen, S. Horiuchi, J. J. Holstein, J. Tessarolo and G. H. Clever, *Chem.–Eur. J.*, 2019, **65**, 14921–14927; (*d*) R. Zhu, W. M. Bloch, J. J. Holstein, S. Mandal, L. V. Schäfer and G. H. Clever, *Chem.–Eur. J.*, 2018, **24**, 12976–12982; (*e*) S. M. Jansze, G. Cecot,

M. D. Wise, K. O. Zhurov, T. K. Ronson, A. M. Castilla, A. Finelli, P. Pattison, E. Solari, R. Scopelliti, G. E. Zelinskii, A. V. Vologzhanina, Y. Z. Voloshin, J. R. Nitschke and K. Severin, *J. Am. Chem. Soc.*, 2016, **138**, 2046–2054; (*f*) D. Preston, J. E. Barnsley, K. C. Gordon and J. D. Crowley, *J. Am. Chem. Soc.*, 2016, **138**, 10578–10585; (*g*) M. D. Wise, J. J. Holstein, P. Pattison, C. Besnard, E. Solari, R. Scopelliti, G. Bricogne and K. Severin, *Chem. Sci.*, 2015, **6**, 1004–1010.

6 E. G. Percástegui, *Eur. J. Inorg. Chem.*, 2021, 4425–4438.

7 For examples, see: (*a*) S. Sudan, F. Fadaei-Tirani, K. E. Ebbert, G. H. Clever and K. Severin, *Angew. Chem., Int. Ed.*, 2022, e202201823; (*b*) T. Tsutsui, L. Catti, K. Yoza and M. Yoshizawa, *Chem. Sci.*, 2020, **11**, 8145–8150; (*c*) T. Zhang, L.-P. Zhou, X.-Q. Guo, L.-X. Cai and Q.-F. Sun, *Nat. Commun.*, 2017, **8**, 15898; (*d*) R. Zhu, J. Lübben, B. Dittrich and G. H. Clever, *Angew. Chem., Int. Ed.*, 2015, **54**, 2796–2800; (*e*) S. Freye, R. Michel, D. Stalke, M. Pawliczek, H. Frauendorf and G. H. Clever, *J. Am. Chem. Soc.*, 2013, **135**, 8476–8479; (*f*) R. Sekiya, M. Fukuda and R. Kuroda, *J. Am. Chem. Soc.*, 2012, **134**, 10987–10997.

8 (*a*) G. H. Clever and P. Punt, *Acc. Chem. Res.*, 2017, **50**, 2233–2243; (*b*) A. Casini, B. Woods and M. Wenzel, *Inorg. Chem.*, 2017, **56**, 14715–14729.

9 For examples of drug encapsulation, see: (*a*) B. Woods, R. D. M. Silva, C. Schmidt, D. Wragg, M. Cavaco, V. Neves, V. F. C. Ferreira, L. Gano, T. S. Morais, F. Mendes, J. D. G. Correira and A. Casini, *Bioconjugate Chem.*, 2021, **32**, 1399–1408; (*b*) R. A. S. Vasdev, L. F. Gaudin, D. Preston, J. P. Jogy, G. I. Giles and J. D. Crowley, *Front. Chem.*, 2018, **6**, 563; (*c*) F. Kaiser, A. Schmidt, W. Heydenreuter, P. J. Altmann, A. Casini, S. A. Sieber and F. E. Kühn, *Eur. J. Inorg. Chem.*, 2016, 5189–5196; (*d*) A. Schmidt, V. Molano, M. Hollering, A. Pöthig, A. Casini and F. E. Kühn, *Chem.–Eur. J.*, 2016, **22**, 2253–2256; (*e*) J. E. M. Lewis, E. L. Gavey, S. A. Cameron and J. D. Crowley, *Chem. Sci.*, 2012, **3**, 778–784.

10 (*a*) R.-J. Li, C. Pezzato, C. Berton and K. Severin, *Chem. Sci.*, 2021, **12**, 4981–4984; (*b*) S.-Q. Deng, D.-M. Li, X.-J. Mo, Y.-L. Miao, S.-L. Cai, J. Fan, W.-G. Zhang and S.-R. Zheng, *ChemPlusChem*, 2021, **86**, 709–715; (*c*) Y. Gao, S.-Q. Deng, X. Jin, S.-L. Cai and S.-R. Zheng, *Chem. Eng. J.*, 2019, **357**, 129–139; (*d*) L. Zeng, Y. Xiao, J. Jiang, H. Fang, Z. Ke, L. Chen and J. Zhang, *Inorg. Chem.*, 2019, **58**, 10019–10027; (*e*) S. Saha, B. Holzapfel, Y.-T. Chen, K. Terlinden, P. Lill, C. Gatsogiannis, H. Rehage and G. H. Clever, *J. Am. Chem. Soc.*, 2018, **140**, 17384–17388; (*f*) Y. Gu, E. A. Alt, H. Wang, X. Li, A. P. Willard and J. A. Johnson, *Nature*, 2018, **560**, 65–69; (*g*) J. Uchida, M. Yoshio, S. Sato, H. Yokoyama, M. Fujita and T. Kato, *Angew. Chem., Int. Ed.*, 2017, **56**, 14085–14089; (*h*) Y. Wang, Y. Gu, E. G. Keeler, J. V. Park, R. G. Griffin and J. A. Johnson, *Angew. Chem., Int. Ed.*, 2017, **56**, 188–192; (*i*) A. V. Zhukhovitskiy, M. Zhong, E. G. Keeler, V. K. Michaelis, J. E. P. Sun, M. J. A. Hore, D. J. Pochan, R. G. Griffin, A. P. Willard and J. A. Johnson, *Nat. Chem.*, 2016, **8**, 33–41; (*j*) A. V. Zhukhovitskiy, J. Zhao, M. Zhong, E. G. Keeler, E. A. Alt, P. Teichen, R. G. Griffin, M. J. A. Hore, A. P. Willard and J. A. Johnson, *Macromolecules*, 2016, **49**, 6896–6902.

11 (*a*) R. Saha, B. Mondal and P. S. Mukherjee, *Chem. Rev.*, 2022, **122**, 12244–12307; (*b*) P. Howlander and M. Schmittel, *Beilstein J. Org. Chem.*, 2022, **18**, 597–630; (*c*) Y. Xue, X. Hang, J. Ding, B. Li, R. Zhu, H. Pang and Q. Xu, *Coord. Chem. Rev.*, 2021, **430**, 213656; (*d*) A. B. Grommet, M. Feller and R. Klajn, *Nat. Nanotechnol.*, 2020, **15**, 256–271; (*e*) A. C. H. Jans, X. Caumes and J. N. H. Reek, *ChemCatChem*, 2019, **11**, 287–297; (*f*) L. J. Jongkind, X. Caumes, A. P. T. Hartendorp and J. N. H. Reek, *Acc. Chem. Res.*, 2018, **51**, 2115–2128; (*g*) I. Sinha and P. S. Mukherjee, *Inorg. Chem.*, 2018, **57**, 4205–4221.

12 L. Tian, C. Wang, H. Zhao, F. Sun, H. Dong, K. Feng, P. Wang, G. He and G. Li, *J. Am. Chem. Soc.*, 2021, **143**, 8631–8638.

13 S. Pullen, J. Tessarolo and G. H. Clever, *Chem. Sci.*, 2021, **12**, 7269–7293.

14 (*a*) C. T. McTernan, J. A. Davies and J. R. Nitschke, *Chem. Rev.*, 2022, **122**, 10393–10437; (*b*) J. E. M. Lewis and J. D. Crowley, *ChemPlusChem*, 2020, **85**, 815–827.

15 (*a*) S. S. Mishra and D. K. Chand, *Dalton Trans.*, 2022, **51**, 11650–11657, DOI: **10.1039/d2dt01571d**; (*b*) R. A. S. Vasdev, D. Preston, C. A. Casey-Stevens, V. Martí-Centelles, P. J. Lusby, A. L. Garden and J. D. Crowley, *Inorg. Chem.*, 2022, DOI: **10.1021/acs.inorgchem.2c00937**; (*c*) A. Tarzia, J. E. M. Lewis and K. E. Jelfs, *Angew. Chem., Int. Ed.*, 2021, **60**, 20879–20887; (*d*) J. E. M. Lewis, *Chem.–Eur. J.*, 2021, **27**, 4454–4460; (*e*) H. Yu, J. Li, C. Shan, T. Lu, X. Jiang, J. Shi, L. Wojtas, H. Zhang and M. Wang, *Angew. Chem., Int. Ed.*, 2021, **60**, 26523–26527; (*f*) J. E. M. Lewis, A. Tarzia, A. J. P. White and K. E. Jelfs, *Chem. Sci.*, 2020, **11**, 677–683; (*g*) S. S. Mishra, S. V. K. Kompella, S. Krishnaswamy, S. Balasubramanian and D. K. Chand, *Inorg. Chem.*, 2020, **59**, 12884–12894; (*h*) S. Samantray, S. Krishnaswarmy and D. K. Chand, *Nat. Commun.*, 2020, **11**, 880; (*i*) S. K. Sen and R. Natarajan, *Inorg. Chem.*, 2019, **58**, 7180–7188; (*j*) D. Ogata and J. Yuasa, *Angew. Chem., Int. Ed.*, 2019, **58**, 18424–18428.

16 R.-J. Li, A. Marcus, F. Fadaei-Tirani and K. Severin, *Chem. Commun.*, 2021, **57**, 10023–10026.

17 B. Kandasamy, E. Lee, D.-L. Long, N. Bell and L. Cronin, *Inorg. Chem.*, 2021, **60**, 14772–14778.

18 D. S. Dummit and R. M. Foote, *Abstract Algebra*, 3rd edn, Wiley-VCH, 2003.

19 W. Y. C. Chen, *SIAM J. Discret. Math.*, 1993, **6**, 353–362.

20 A. Tarzia, J. E. M. Lewis and K. E. Kelfs, *Angew. Chem., Int. Ed.*, 2021, **60**, 20879–20887.

21 L. Turcani, A. Tarzia, F. T. Szczypiński and K. E. Kelfs, *J. Chem. Phys.*, 2021, **154**, 214102.

22 (*a*) **https://github.com/lukasturcani/stk**, version2022.1.26.0; (*b*) *The Python code for the computational model generation is open-source at*, **https://github.com/andrewtarzia/big_unsymm**.

23 (*a*) D. E. Coupry, M. A. Addicoat and T. Heine, *J. Chem. Theory Comput.*, 2016, **12**, 5215–5225; (*b*) M. A. Addicoat, N. Vankova, I. F. Aktera and T. Heine, *J. Chem. Theory*

Comput., 2014, **10**, 880–891; (*c*) J. D. Gale and A. L. Rohl, *Mol. Simul.*, 2003, **29**, 291–341; (*d*) J. D. Gale, *J. Chem. Soc., Faraday Trans.*, 1997, **93**, 629–637; (*e*) A. K. Rappe, C. J. Casewit, K. S. Colwell, W. A. Goddard III and W. M. Skiff, *J. Am. Chem. Soc.*, 1992, **114**, 10024–10035.

24 (*a*) C. Bannwarth, E. Caldeweyher, S. Ehlert, A. Hansen, P. Pracht, J. Seibert, S. Spicher and S. Grimme, *Wires Comput. Mol. Sci.*, 2021, **11**, e1493; (*b*) C. Bannwarth, S. Ehlert and S. Grimme, *J. Chem. Theory Comput.*, 2019, **15**, 1652–1671.

25 (*a*) S. Grimme, S. Ehrlich and L. Goerigk, *J. Comput. Chem.*, 2011, **32**, 1456–1465; (*b*) C. Adamo and V. Barone, *J. Chem. Phys.*, 1999, **110**, 6158–6170.

26 (*a*) J. Heyd, G. E. Scuseria and M. Ernzerhof, *J. Chem. Phys.*, 2006, **124**, 219906; (*b*) J. Heyd, G. E. Scuseria and M. Ernzerhof, *J. Chem. Phys.*, 2006, **124**, 219906.

27 F. Weigend and R. Ahlrichs, *Phys. Chem. Chem. Phys.*, 2005, **7**, 3297–3305.

28 The crystallographic analysis suggests the presence of chloride instead of nitrate counter ions. The origin of the chloride anions is not clear. Potentially, anion exchange with the glassware had occurred over the very long crystallization period (several months), or small amounts of chloride were present in the $Pd(NO_3)_2$ salt. For a related discussion, see: E. O. Bobylev, B. De Bruin and J. N. H. Reek, *Inorg. Chem.*, 2021, **60**, 12498–12505.

29 O. V. Dolomanov, J. L. Bourhis, R. J. Gildea, J. A. K. Howard and H. Puschmann, *J. Appl. Crystallogr.*, 2009, **42**, 339–341.

30 For examples, see: (*a*) R. Zaffaroni, E. O. Bobylev, R. Plessius, J. I. van der Vlugt and R. N. H. Reek, *J. Am. Chem. Soc.*, 2020, **142**, 8837–8847; (*b*) C.-L. Liu, E. O. Bobylev, Y. Fu, D. A. Poole III, K. Robeyns, C.-A. Fustin, Y. Garcia, J. N. H. Reek and M. L. Singleton, *Chem.–Eur. J.*, 2020, **26**, 11960–11965; (*c*) S. Gonell, X. Caumes, N. Orth, I. Ivanović-Burmazović and J. N. H. Reek, *Chem. Sci.*, 2019, **10**, 1316–1321; (*d*) S. Sato, M. Ikemi, T. Kikuchi, S. Matsumura, K. Shiba and M. Fujita, *J. Am. Chem. Soc.*, 2015, **137**, 12890–12896; (*e*) C. J. Bruns, D. Fujita, M. Hoshino, S. Sato, J. F. Stoddart and M. Fujita, *J. Am. Chem. Soc.*, 2014, **136**, 12027–12034; (*f*) C. Gütz, R. Hovorka, C. Klein, Q.-Q. Jiang, C. Bannwarth, M. Engeser, C. Schmuck, W. Assenmacher, W. Mader, F. Topíc, K. Rissanen, S. Grimme and A. Lützen, *Angew. Chem., Int. Ed.*, 2014, **53**, 1693–1698; (*g*) F. Jiang, N. Wang, Z. Du, J. Wang, Z. Lan and R. Yang, *Chem.–Asian J.*, 2012, **7**, 2230–2234; (*h*) K. Suzuki, M. Kawano, S. Sato and M. Fujita, *J. Am. Chem. Soc.*, 2007, **129**, 10652–10653; (*i*) T. Murase, S. Sato and M. Fujita, *Angew. Chem., Int. Ed.*, 2007, **46**, 1083–1085; (*j*) S. Sato, J. Iida, K. Suzuki, M. Kawano, T. Ozeki and M. Fujita, *Science*, 2006, **313**, 1273–1276; (*k*) M. Tominaga, K. Suzuki, T. Murase and M. Fujita, *J. Am. Chem. Soc.*, 2005, **127**, 11950–11951; (*l*) M. Tominaga, K. Suzuki, M. Kawano, T. Kusukawa, T. Ozeki, S. Sakamoto, K. Yamaguchi and M. Fujita, *Angew. Chem., Int. Ed.*, 2004, **43**, 5621–5625.

31 (*a*) M. Han, Y. Luo, B. Damaschke, L. Gómez, X. Ribas, A. Jose, P. Peretzki, M. Seibt and G. H. Clever, *Angew. Chem., Int. Ed.*, 2016, **55**, 445–449; (*b*) H. Yokoyama, Y. Ueda, D. Fujita, S. Sato and M. Fujita, *Chem.–Asian J.*, 2015, **10**, 2292–2295; (*c*) J. Bunzen, J. Iwasa, P. Bonakdarzadeh, E. Numata, K. Rissanen, S. Sato and M. Fujita, *Angew. Chem., Int. Ed.*, 2012, **51**, 3161–3163.

32 The crystallographic analysis of a $[Cu_6L_{12}]^{12+}$ cage with bridging 3-pyridinyl-triazole ligands showed also exclusive *cis* coordination at the six metal centers: Y. Wang, P. Cheng, Y. Song, D.-Z. Liao and S.-P. Yan, *Chem.–Eur. J.*, 2007, **13**, 8131–8138.